Title

Distribution of mercury species in the Western Arctic Ocean (U.S. GEOTRACES GN01)

Authors

Agather, Alison M
Bowman, Katlin L
Lamborg, Carl H
et al.

Publication Date

2019-10-01

DOI

10.1016/j.marchem.2019.103686

Peer reviewed

Marine Chemistry 216 (2019) 103686

Contents lists available at ScienceDirect

Marine Chemistry

journal homepage: www.elsevier.com/locate/marchem

Distribution of mercury species in the Western Arctic Ocean (U.S. GEOTRACES GN01)

Alison M. Agather[a,*,1], Katlin L. Bowman[b], Carl H. Lamborg[b], Chad R. Hammerschmidt[a]

[a] Department of Earth & Environmental Sciences, Wright State University, Dayton, OH 45435, United States of America
[b] Department of Ocean Sciences, University of California Santa Cruz, Santa Cruz, CA 95064, United States of America

ARTICLE INFO

Keywords:
Mercury
Monomethylmercury
Transpolar drift
GEOTRACES

ABSTRACT

Mercury (Hg) in the Arctic Ocean is a concern due to unusually high concentrations of monomethylmercury (MMHg) in fish and marine animals. Increased human exposure from consumption of these animals is a significant health concern that is related to Hg contamination in nature. Most Arctic marine Hg research has investigated the amounts, distributions, and cycling in animals, snow, and ice, while few studies have examined the aqueous behavior and fate of Hg in the polar ocean. Here we present the most comprehensive dataset published to date detailing Hg speciation and distribution of elemental Hg (Hg^0), dimethylmercury (DMHg), and filtered and particulate total Hg and MMHg in the western Arctic Ocean. This data was obtained as part of the U.S. Arctic GEOTRACES cruise (GN01) in 2015. Many water masses sampled appeared to be enriched with anthropogenic Hg. The Transpolar Drift supplied HgT and Hg^0 to the central Arctic Ocean, but not methylated Hg. Gaseous Hg^0, but not DMHg, was elevated in surface waters under the ice cover. Monomethylmercury levels, which averaged 0.054 ± 0.050 pM, are lower than other major ocean basins, suggesting ambient MMHg levels in western Arctic Ocean seawater do not by themselves explain anomalously high Hg in Arctic animals.

1. Introduction

Monomethylmercury (MMHg) is a bioaccumulating neurotoxin that, at current environmental exposures, poses a health risk to humans (Mergler et al., 2007) and wildlife (Scheuhammer et al., 2015). Human exposure to MMHg is primarily from seafood consumption (Sunderland, 2007), and the rate and quantity of seafood consumed may predict which individuals and populations are adversely affected by MMHg exposure (Grandjean et al., 1995; Ha et al., 2017; Karagas et al., 2012; Mahaffey et al., 2009; Mergler et al., 2007; Sheehan et al., 2014; Van Oostdam et al., 2005). Exposures of women of child-bearing age are of particular concern because MMHg can be maternally transferred to their children while in utero and nursing (Mergler et al., 2007; Oskarsson et al., 1996). Arctic populations have an increased risk of accumulating high levels of MMHg. Concentrations of mercury (Hg), mostly as MMHg, in Arctic animals are often greater than those in animals of similar trophic status at lower latitudes (Dietz et al., 1998; Dietz et al., 2009). There are contrasting hypothesis regarding the relationship between MMHg accumulation and temperature. Some data suggests Hg accumulation per trophic level is highest at low temperatures (Lavoie et al., 2013), while other results indicate single organisms accumulate more Hg at higher temperatures (Dijkstra et al., 2013). Mechanisms responsible for exacerbated MMHg in Arctic biota are unknown, although many factors have been hypothesized to contribute to the complex cycling of Hg in the Arctic, including atmospheric Hg depletion events (Lindberg et al., 2002; Schroeder et al., 1998; Steffen et al., 2007), presence of snow pack (Kirk et al., 2006; St. Louis et al., 2007) and sea ice (Beattie et al., 2014), potential for Hg methylation in ice brine (Gionfriddo et al., 2016), and methylation in the stratified polar mixed layer (Heimbürger et al., 2015; Lehnherr et al., 2011; Schartup et al., 2015; Wang et al., 2018).

Exacerbating these unique Arctic Hg cycling mechanisms are anthropogenic Hg emissions. The relatively long atmospheric residence time of Hg (~ 0.5–1 year, Horowitz et al., 2017; Slemr et al., 1985) coupled to its tendency to re-volatize following deposition allows for long range transport of the contaminant before it is deposited (Fitzgerald et al., 1998; Mason et al., 2012; Slemr and Langer, 1992; Swain et al., 1992). There are no large point sources of Hg in the Arctic,

* Corresponding author.
E-mail addresses: agather.2@wright.edu (A.M. Agather), klbouman@ucsc.edu (K.L. Bowman), clamborg@ucsc.edu (C.H. Lamborg), chad.hammerschmidt@wright.edu (C.R. Hammerschmidt).
[1] Present address: 3640 Colonel Glenn Hwy., 260 Brehm Lab, Dayton, OH 45435, USA
T: 952-220-9657.

https://doi.org/10.1016/j.marchem.2019.103686
Received 10 September 2018; Received in revised form 10 May 2019; Accepted 4 July 2019
Available online 05 July 2019
0304-4203/

however, atmospheric transport of elemental Hg (Hg^0) to the region is a significant source of the metal (Outridge et al., 2008). Emissions from human activities since the Industrial Revolution have increased Hg deposition in the Arctic by a factor of three (Fitzgerald et al., 1998; Fitzgerald et al., 2005). Mercury levels in Arctic animals have increased over the same period of time, 92% of which has been attributed to anthropogenic emissions (Dietz et al., 2009). Unlike other ocean basins, Arctic Ocean mass balance estimates suggest that sources other than atmospheric deposition may be important, including rivers, melting permafrost, and exchange with the Pacific and Atlantic Oceans (Dastoor and Durnford, 2014; Outridge et al., 2008; Soerensen et al., 2016; Zhang et al., 2015). These sources supply Hg to the oceanic water column, where it undergoes a complex series of biotic and abiotic reactions, forming dissolved Hg^0, MMHg and dimethylmercury (DMHg).

A series of hypotheses have attempted to address the difference between Hg cycling in the Arctic Ocean and other basins. Atmospheric depletion events are unique to polar regions and are a large source of Hg(II) to the Arctic environment (Schroeder et al., 1998; Steffen et al., 2007). Riverine discharge provides another significant supply of Hg entering the Arctic (Fisher et al., 2012), and both of these sources are frequently used to explain recent biotic Hg trends. Delivery of Hg into the Arctic Ocean is worsened by climate change and thawing permafrost, which supplements already substantial riverine Hg loads (Fisher et al., 2013; Soerensen et al., 2016; Schuster et al., 2018). Warming air and sea temperatures likely affect Hg cycling between the ocean, atmosphere and sea ice (Outridge et al., 2008). Ice-free waters increase vertical mixing which brings MMHg and DMHg to the surface. After mixing, DMHg can efflux from the surface ocean into the atmosphere and be deposited as MMHg (Baya et al., 2015; Kirk et al., 2008; St. Louis et al., 2007; St. Pierre et al., 2015). Mixing also brings MMHg to the surface ocean, where it is likely to enter the food chain (Kirk et al., 2008). And while it has not been directly addressed in the Arctic, MMHg accumulation in temperate coastal food webs can largely be attributed to methylation in near-shore and shelf sediments (Hammerschmidt et al., 2004; Hammerschmidt and Fitzgerald, 2006a), which may be important over the vast Arctic shelves.

Yet still, a lack of sufficient ocean data adjudicate these hypotheses. To better understand Hg cycling in the Arctic Ocean, we measured filtered gaseous Hg^0 and DMHg, filtered total Hg (HgT) and MMHg, and particulate total Hg (HgT_{Part}) and MMHg ($MMHg_{Part}$) in the western Arctic Ocean. This U.S. GEOTRACES transect (GN01) was part of the first large-scale effort to examine Hg speciation and distribution in the Arctic Ocean. Contemporaneous GEOTRACES cruises were conducted in the Canadian Arctic Archipelago and in the eastern Arctic Ocean. Here, we present results of the U.S. GEOTRACES cruise in the western Arctic Ocean.

2. Methods

2.1. Sampling

Water and particles were sampled between August 9th and October 12th, 2015 during the U.S. Arctic GEOTRACES (GN01) section (Fig. 1). The section began in the Bering Sea and passed through the Bering Strait, traversed the Makarov Basin, reached the North Pole (Eurasian Basin), and returned southeast through the Canada Basin. Water samples were collected by deploying a trace-metal clean rosette attached to a plastic-coated hydrowire fitted with 12-L Teflon-coated GO-Flo bottles (Cutter and Bruland, 2012). Water was sampled at twenty-two full depth stations (24 depths) and five marginal ice zone stations (MIZ, 3–5 depths). The MIZ was identified as the region where sea ice was loose and broken. Immediately following rosette recovery, GO-Flo bottles were transferred to a clean laboratory van, and filtered (0.2 μm Pall AcroPak-200) without degassing into 2-L Teflon bottles for Hg^0, MMHg, and DMHg analysis (Lamborg et al., 2012); and into 0.25-L borosilicate glass bottles for HgT analysis. Sample bottles were acid cleaned (Hammerschmidt et al., 2011) and trace-metal clean techniques were followed (Bishop et al., 2012). In addition to GO-Flo samples, seawater from six stations was sampled at 1, 5 and 20 m below the ice with a pump and acid washed plastic tubing. Under-ice samples were collected from on top of an ice floe, pumped under the protection of a tent and upwind of the ship. Seawater collected this way was filtered (0.2 μm Pall AcroPak-200) in a clean lab on board the ship and dispensed into clean bottles for Hg analysis.

Suspended particles (1–51 μm) were sampled from 16 depths at 20 stations with McLane in situ pumps (Bishop et al., 2012; Whatman QMA). Filters were subsampled in two 13 mm diameter punches and stored frozen until analysis (Bowman et al., 2015). The total volume of filtered seawater varied between 16 and 164 L, with larger volumes generally collected at deeper depths.

2.2. Mercury analysis

Elemental Hg, DMHg, and HgT were measured in a shipboard laboratory. Within two hours of collection, samples were purged with Hg-free N_2 gas to quantitatively strip Hg^0 and DMHg from solution (Bowman and Hammerschmidt, 2011). Bond Elut ENV (Agilent; Baya et al., 2013) traps were used to concentrate DMHg from effluent upstream of Hg^0-collecting gold traps (Bloom and Fitzgerald, 1988; Bowman et al., 2016). Elemental Hg was quantified by dual Au-amalgamation cold vapor atomic fluorescence spectrometry (CVAFS; Bloom and Fitzgerald, 1988), with a method detection limit of 0.04 pM. When extra water was available, duplicate samples were analyzed for Hg^0, with a relative percent difference (RPD) of 14 ± 11 (n = 8). In contrast to previous U.S. GEOTRACES cruises, DMHg was not analyzed by gas chromatographic-CVAFS; (Baya et al., 2013; Bloom, 1989; Bowman and Hammerschmidt, 2011; Bowman et al., 2015; Bowman et al., 2016), because the cold temperature of the compressed argon (stored on deck) resulted in insufficient pressure in the gas chromatographic column. Instead, DMHg was thermally desorbed from the Bond Elut traps, thermally decomposed to Hg^0, collected on an in-line Au trap, and quantified via CVAFS. Calibration of at-sea measurements of Hg^0, HgT, and DMHg were performed with gaseous Hg^0 standards. Trapping efficiency for each analytical Bond Elut trap was determined with an ethylated MMHg standard (methylethylmercury; Bowman and Hammerschmidt, 2011), that was validated against TORT-2 reference material (lobster hepatopancreas, Canadian Research Council). The method detection limit for DMHg was 0.012 pM, and duplicates averaged 15 ± 5 RPD (n = 4).

Seawater for analysis of total Hg was oxidized with bromine monochloride (BrCl; Bloom and Crecelius, 1983) and neutralized with NH_2OH prior to reduction with $SnCl_2$. Samples were quantified by dual Au-amalgamation CVAFS (Bloom and Fitzgerald, 1988; Fitzgerald and Gill, 1979). The method detection limit for HgT was 0.10 pM. Reproducibility between analytical duplicates averaged 11 ± 5 RPD (n = 17).

While at sea, variable gas pressure in the gas chromatograph caused irregular MMHg peak retention times, making it indecipherable from the inorganic Hg peak. Accordingly, after purging Hg^0 and DMHg from the samples, samples ranging from 0.25 to 2 L were acidified to 1% with sulfuric acid and shipped frozen to Wright State University for analysis. Samples were thawed > 12 h in the dark at room temperature, acidity neutralized with KOH, buffered with acetate, amended with ascorbic acid (Munson et al., 2014), derivatized with sodium tetraethylborate, and analyzed via flow injection GC-CVAFS (Bowman and Hammerschmidt, 2011; Tseng et al., 2004). The method detection limit was 0.025 pM MMHg for 0.22-L and 0.020 pM MMHg for 0.4-L samples. Agreement between analytical replicates averaged 11 ± 8 RPD (n = 5).

Particulate samples were digested in 2 N HNO_3 in a 60 °C water bath for 12 h (Hammerschmidt and Fitzgerald, 2006b). Aliquots of the digestate (5-mL) were analyzed for particulate MMHg by flow- injection

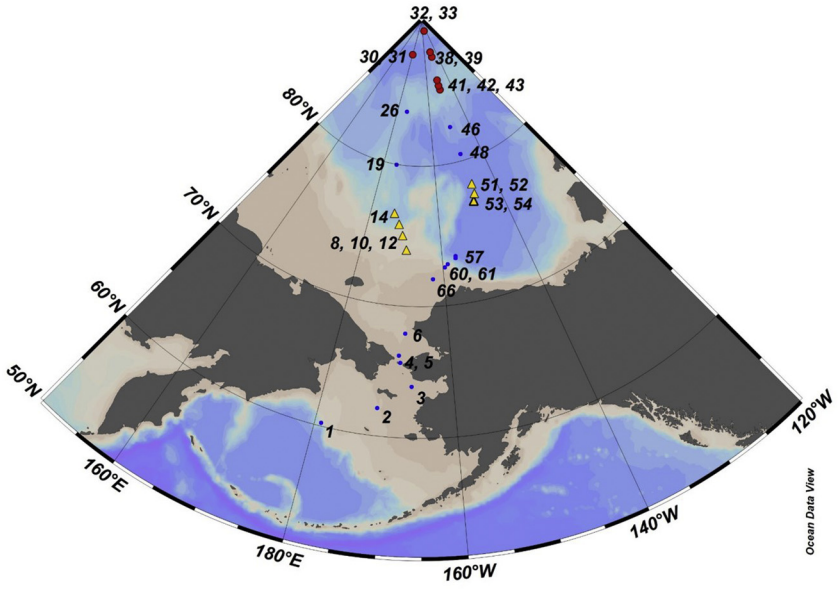

Fig. 1. Water-sampling stations along the U.S. GEOTRACES western Arctic section (GN01). Transpolar drift (TPD) stations denoted by red dots and marginal ice zone (MIZ) stations are indicated with yellow triangles. Stations north of the MIZ were ice covered, while stations south of the MIZ were ice-free. (For interpretation of the references to colour in this figure legend, the reader is referred to the web version of this article.)

GC-CVAFS (Bowman et al., 2015; Tseng et al., 2004). Sample measurements were calibrated against similarly digested MMHg standards, which were validated versus digestates of TORT-2 reference material (lobster hepatopancreas, Canadian Research Council). For particulate HgT, 2-mL aliquots of the same filter digestates were oxidized with BrCl for > 12 h. Samples were neutralized with NH_2OH, reduced with $SnCl_2$, and analyzed via CVAFS that was calibrated with aqueous Hg(II) standards traceable to the U.S. National Institute of Standards and Technology (Bloom and Fitzgerald, 1988). The estimated detection limits for analysis of $MMHg_{Part}$ and HgT_{Part} were 0.002 and 0.02 pM, respectively, agreement between analytical replicates of HgT_{Part} averaged 7 ± 6 RPD (n = 16). Insufficient volume and low sample concentration did not allow for $MMHg_{Part}$ duplicates. Statistical comparisons between water masses were performed with Mann-Whitney Rank Sum Test.

3. Results and discussion

3.1. Physical oceanography

The Arctic Ocean is the smallest (1.56×10^7 km^2) and shallowest (mean depth = 1200 m) ocean basin, characterized by broad continental shelves contributing to 53% of its area (Jakobsson, 2002). Salty waters enter the Arctic Ocean from both sides of Greenland, while fresher North Pacific water flows through the Bering Strait. The ocean basin is split by the Lomonsov Ridge, separating the Canadian Basin (max depth ~3800 m) from the Eurasian Basin (max depth ~4200 m; Rudels, 2001). Subdivisions of the Canadian Basin include the Makarov and Canada Basins, while the Eurasian Basin is subdivided into the Nansen and Amundsen Basins.

The water column of the Arctic Ocean can be divided into three distinct density layers. Polar Surface Water (PSW; $\sigma_\theta \leq 27.70$) consists of the fresh Polar Mixed Layer (PML, < 51 m depth) and the halocline (Fig. 2). The intermediate layer ($27.70 < \sigma_\theta > 30.444$) is composed of Atlantic Water (AW) and upper Polar Deep Water (uPDW). Deep water ($\sigma_\theta > 30.444$) results from slope convection and is differentiated on either side of the Lomonsov Ridge as Eurasian Basin Deep Water (EBDW) and Canada Basin Deep Water (CBDW; Rudels, 2001).

Circulation in the Arctic Ocean varies by depth. In surface and intermediate layers, rim currents dictate water movement. Surficial flow is cyclonic in the Eurasian Basin and anticyclonic in the Beaufort Gyre in the Canadian Basin. Atmospheric high pressure over the Beaufort Sea drives the Transpolar Drift (TPD), which flows from the Laptev and East Siberian Seas to the Fram Strait, along a similar path as the Lomonosov Ridge (Rudels, 2001). The TPD bisects the Arctic, shuttling ice, Siberian shelf and river water laden with nutrients and trace metals across the basin and out through the Fram Strait (Barrie et al., 1998; Gordienko and Laktionov, 1969; Klunder et al., 2012), though the exact path of the TPD varies year to year due to the Arctic Oscillation index (Macdonald et al., 2005). Intermediate waters move cyclonically throughout the basin, with individual cyclonic cells in the Makarov, Canada, Nansen, and Amundsen Basins. Similar to intermediate layers, deep water circulation is also cyclonic, but the Lomonosov Ridge impedes a continuous rim current (Talley et al., 2011).

Riverine discharge to the Arctic Ocean delivers freshwater, nutrients, metals and carbon. Although the Arctic Ocean comprises only 1.4% of the world ocean volume (Jakobsson, 2002), it receives 11% of global riverine discharge (Lammers et al., 2001). Pan-arctic rivers drain 22.4×10^6 km^2 of land, an area of about one and a half times the size of the Arctic Ocean (Lammers et al., 2001). Rivers average an annual runoff of 3200 km^3 per year, and most of their discharge (46–66%) occurs during the spring freshet (Lammers et al., 2001; McClelland et al., 2006). Although these data provide a good estimate of riverine inflow, overall Arctic river discharge has increased since 1932, and is expected to continue to increase with climate change (McClelland et al., 2006; Peterson et al., 2002).

Sea ice differentiates the Arctic Ocean from other basins. First-year ice forms in late summer in regions of open water, while multi-year ice lasts year round. Multi-year ice exists in the central Arctic, Canadian Basin and around Greenland. Outside the central Arctic, ice consists of more first- than multi-year ice. The outer region of the first-year ice makes up the Marginal Ice Zone (MIZ), where broken ice attenuates wave energy, leading to upwelling, eddies, and jets. The MIZ typically has higher rates of primary production than surrounding water (Talley et al., 2011).

Water along the GN01 transect in the Bering Strait, Makarov and Canada Basins is influenced by inflow from the Pacific and Atlantic Oceans. With the exception of the TPD, surface water throughout this section of the western Arctic Ocean originated from the Pacific Ocean, entering through the Bering Strait as Bering Strait Modified Water (BSMW), which is characterized as having lower salinity with increased silicate and nutrients. Nutrient enrichment results from riverine discharge and inputs from the shelf. In contrast to water from the Pacific, Atlantic water is colder with a higher oxygen content. The surface water sampled from above 85°N (Stations 30–43) was relatively young meteoric water with transport time of 0.5–1 year, and hypothesized to be

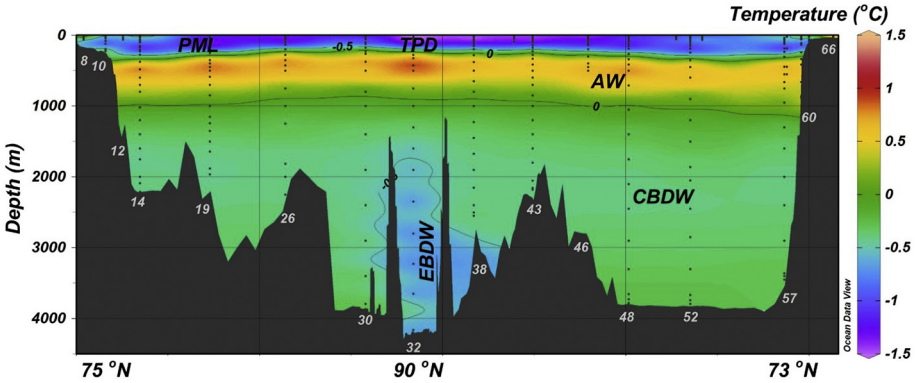

Fig. 2. Water temperature in the GN01 Arctic section, with 0 and − 0.5 °C contour lines noted. Water masses sampled are labeled, including: Polar Mixed Layer (PML), Atlantic Water (AW), Canada Basin Deep Water (CBDW), and Eurasian Basin Deep Water (BDW). The Transpolar Drift (TPD) is also indicated, extending from station 30 to station 43 in the surface layer. Station numbers are indicated in grey numbering along the bathymetry.

transported to the central Arctic Ocean from the East Siberian Arctic Shelf by the TPD (Kipp et al., 2018).

3.2. Filtered total Hg

Filtered HgT in seawater along the Arctic GN01 section ranged from 0.21 to 3.69 pM, and averaged 0.86 ± 0.45 pM among all depths and locations (n = 338; Table 1). Throughout the section, the highest average concentrations of HgT were in the Bering Sea and Strait (1.06 ± 0.59 pM, n = 31; Fig. 3A) and over the Chukchi shelf (1.06 ± 0.60 pM, n = 47, where "shelf" stations have a water depth < 200 m). Water on the Chukchi shelf is more likely to be influenced by sediment resuspension and continental inputs, such as thawing permafrost, of HgT as riverine input was insignificant along the GN01 section in the Chukchi Sea.

Filtered HgT in the PML was variable, ranging from 0.41 to 2.9 pM. There was no HgT enrichment in the ice-covered PML when compared to surface water elsewhere in the section and sea ice (DiMento et al., 2019). However, greater amounts of HgT were measured in the TPD (1.36 ± 0.38 pM, n = 21) than in the ice-capped PML (0.89 ± 0.27 pM n = 13; p < 0.001). A relationship between HgT and fraction of meteoric water (derived from $\delta^{18}O$, Fig. 4, Pasqualini et al., 2017) suggests that HgT in Arctic meteoric water is 4.0 ± 1.7 pM. This estimate is within the range of HgT measurements in Arctic sea ice (0.7–60.8 pM, unfiltered; Beattie et al., 2014) and Russian river water (0.7–13.3 pM; Coquery et al., 1995), but less than Arctic Alaskan rainwater (5–130 pM; Fitzgerald et al., 2005). It is unlikely that increased HgT in meteoric water is due to ice melt, because $\delta^{18}O$ values indicate brine formation rather than freshening of the surface waters (Pasquilini et al., 2017). Thus, if the HgT in meteoric water is not fully explained by Arctic rivers and melting sea ice and associated snow, then vertical mixing over the thawing East Siberian Shelf, as hypothesized by Kipp et al. (2018) for ^{228}Ra, may be the source of increased HgT in the TPD.

Although Arctic deep waters (> 2000 m) along the GN01 section had increased HgT near the sediments, average concentrations were lower than either deep Atlantic or Pacific Ocean waters (Bowman et al., 2015; Bowman et al., 2016; Laurier et al., 2004; Mason et al., 1998; Munson et al., 2015; Table 1). Filtered and particulate HgT increased near the sediment at stations 14, 19, 26, 30, and 52 (Fig. 5), which suggests some vertical mixing with an efflux of HgT from the sediment. Similarly, aluminum concentrations were greater near the bottom, and may also be resuspended from the sediments (Hatta and Measures, 2018). Sediments may be a localized source of HgT to deep Arctic waters, but deep water averages remain low. Increased HgT at the sediment-water interface was observed in the Atlantic and Pacific oceans (Bowman et al., 2015; Bowman et al., 2016). Bottom water HgT in the Canada (0.58 ± 0.24 pM; n = 38) and Eurasian Basins (0.50 ± 0.16 pM; n = 6) did not differ significantly (p = 0.442). These levels are in marked contrast to those in young North Atlantic Deep Water (1.04 ± 0.17 pM; Bowman et al., 2015), modified Pacific Deep Water (1.25 ± 0.23 pM, Bowman et al., 2016), and Antarctic Bottom Water in the Southern Ocean (1.35 ± 0.39 pM; Cossa et al., 2011). Deep water in the Canada and Eurasian Basins was last ventilated about 450 and 240 years ago, respectively (Schlosser et al., 1997). As such, based solely on age, these deep water masses are unlikely to contain much anthropogenic Hg. Sinking particles may add anthropogenic Hg to these water masses, however, due to low primary productivity, we would expect particle-driven sinking of anthropogenic Hg to be low. Thus, compared to other oceans, decreased particle pumping and little pollution enhancement in the Arctic Ocean leads to lower HgT in deep water.

Many of the shallow Arctic Ocean water masses within the GN01 section have the fingerprint of anthropogenic Hg. According to Lamborg et al. (2014), water masses unaffected by anthropogenic Hg inputs have a ratio of HgT to remineralized phosphate (P_{remin}, Apparent Oxygen Utilization divided by 170; Anderson and Sarmiento, 1994), equal to 1.02×10^{-6}. By extension, water masses with a HgT:P_{remin} ratio greater than 1.02×10^{-6} contain anthropogenic Hg. HgT:P_{remin} ratios in the upper Arctic Ocean are about double this ratio and suggest that Hg emissions over the last 300 years have increased Hg concentrations (Fig. 6). Of the water masses sampled, BSMW

Table 1
Summary of filtered and particulate species in the GN01 section, compared to average values from the Atlantic Ocean ([a]Bowman et al., 2015, [b]Mason et al., 1998), Pacific Ocean (Bowman et al., 2016), Mediterranean Sea (Cossa et al., 2009), and Southern Ocean (Cossa et al., 2011).

Hg Species	Mean ± SD (pM)	Range (pM)	n	Atlantic Ocean (pM)	Pacific Ocean (pM)	Mediterranean Sea (pM)	Southern Ocean (pM)
Total Hg	0.86 ± 0.45	0.21–3.69	338	0.89 ± 0.31[a] 2.4 ± 1.6[b]	0.78 ± 0.41	1.19 ± 0.48	1.33 ± 0.45
Hg0	0.20 ± 0.16	< DL–1.03	269	0.48 ± 0.31[b]	0.045 ± 0.061	–	–
MMHg	0.054 ± 0.050	< DL–0.36	164	0.095 ± 0.098[a]	0.07 ± 0.06	–	–
DMHg	0.040 ± 0.029	< DL–0.23	199	0.18 ± 0.12[a] 0.07 ± 0.04[a]	0.07 ± 0.07	–	–
Particulate HgT	0.1 ± 0.1	< DL–0.75	141	0.038 ± 0.039[a] 0.035 ± 0.02[b]	0.075 ± 0.094	–	–
Particulate MMHg	0.004 ± 0.003	< DL–0.011	17	0.0007 ± 0.001[a]	0.0007 ± 0.001	–	–

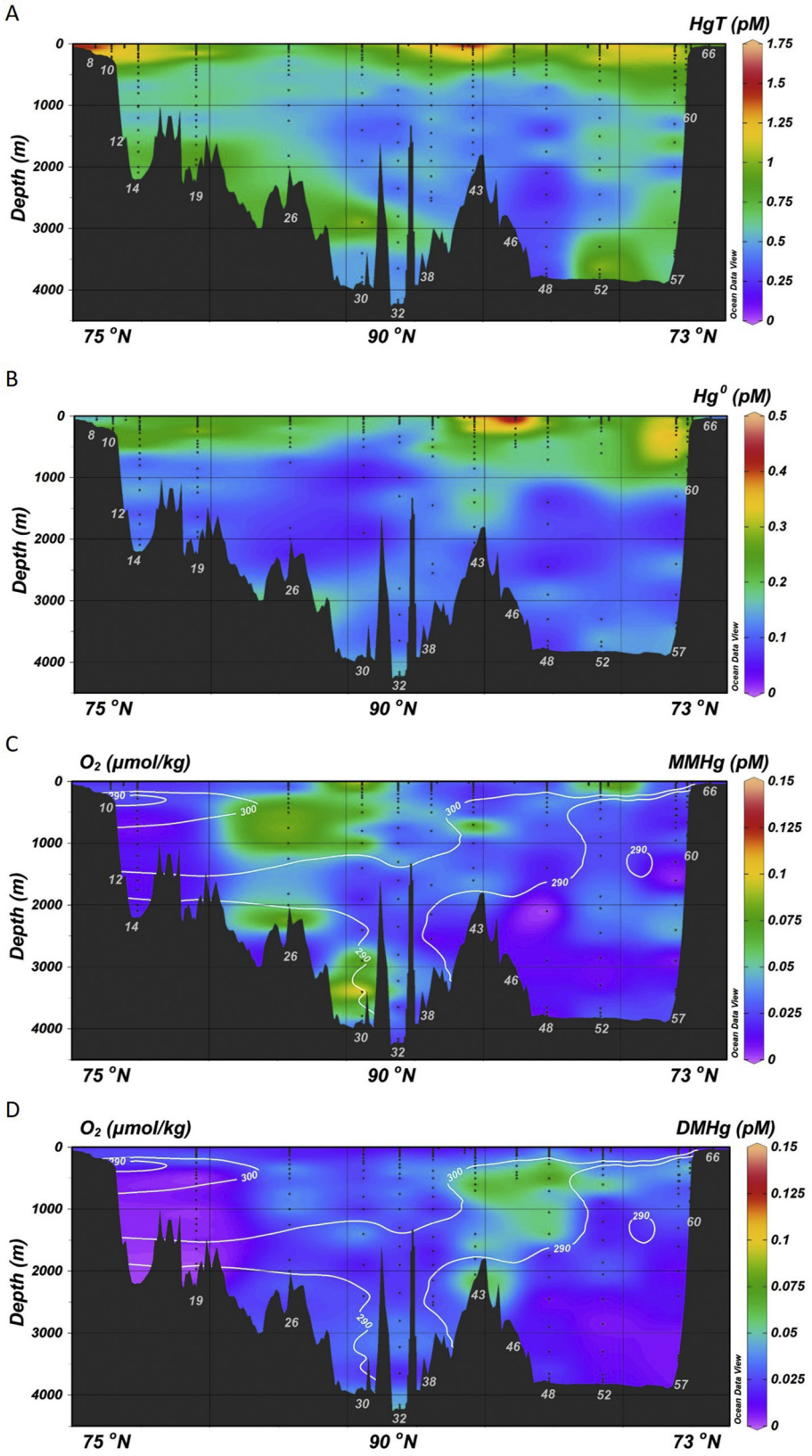

Fig. 3. Filtered total Hg (HgT, A), elemental Hg (Hg^0, B), monomethyl-Hg (MMHg, C), and dimethyl-Hg (DMHg, D) in the western Arctic Ocean. Dots indicate water sample depth, and the numbers listed in the bathymetry indicate station number.

(2.8 ± 2.4 × 10^{-6}) and ATL (2.4 ± 0.5 × 10^{-6}) contained more HgT than would be expected from remineralization of pre-industrial particulate matter alone. Water sampled from EBDW (1.4 ± 0.1 × 10^{-6}) and CBDW (1.5 ± 0.2 × 10^{-6}) was above the 95% confidence interval, suggesting the water masses have extra HgT. Deep waters in both the Canada and Eurasian Basins exhibit the least amount of

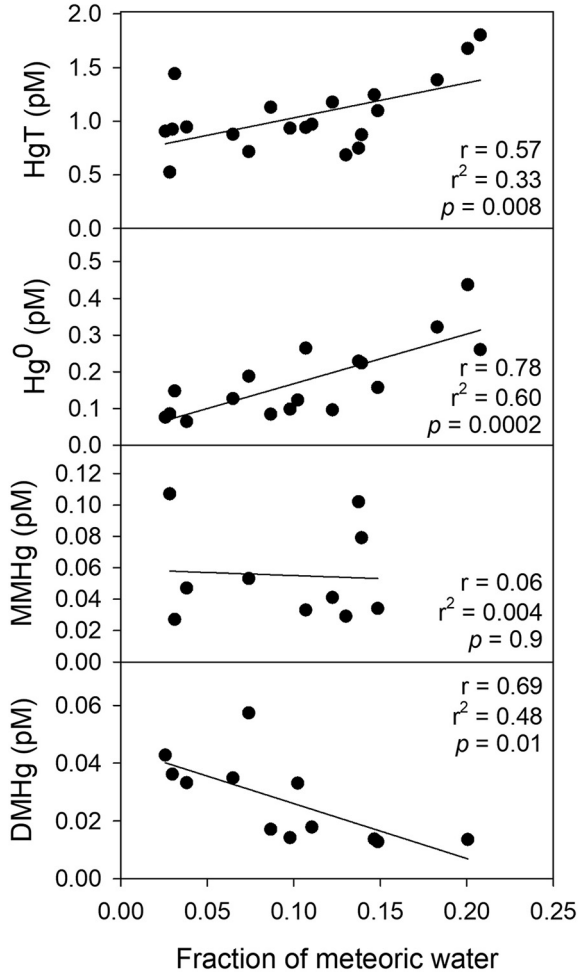

Fig. 4. HgT, Hg^0, MMHg and DMHg plotted versus the fraction of meteoric water in the upper 100 m of stations above 85°N (Stations 30–43), in the Transpolar Drift (Pasqualini et al., 2017). The regression for MMHg is not significant. The equation from the HgT regression line, y = 3.2569 x + 0.7062, can be used to extrapolate HgT content in 100% meteoric water.

anthropogenic impact, with ~1.4 times the amount of Hg we would expect from remineralization alone. As previously discussed, sediment resuspension supplies deep Arctic waters with Hg, however, it is unlikely this process impacts the entirety of the deep water masses.

Pacific water entering the Bering Strait contains about the same concentration of HgT leaving the Strait. Previous research from the VERTEX (1986–1987) and IOC cruises (2002) reported unfiltered HgT concentrations of 0.58 ± 0.37 pM and 0.64 ± 0.26 pM in North Pacific upper water (Laurier et al., 2004). If we assume these upper waters entered the Bering Strait without much alteration to HgT content, and compare these values to our Bering Strait upper water column mean of 1.3 ± 0.81 pM (sum of filtered and particulate HgT), there has not been an increase of HgT entering the Arctic Ocean from the North Pacific over the last two decades. From concentrations measured in this study and an estimate of Pacific inflow of 0.83 ± 0.66 Sv (Roach et al., 1995), we estimate the range of HgT entering the Arctic Ocean from the Bering Strait to be 4–71 kmol yr^{-1}. This range encompasses previous estimates of 20 kmol yr^{-1} (Outridge et al., 2008) and 27.5 kmol yr^{-1} (Soerensen et al., 2016). However, the flux of HgT into the Arctic Ocean from the Bering Strait is small source compared to other sources (Outridge et al., 2008; Soerensen et al., 2016).

3.3. Elemental Hg

Filtered Hg^0 in the Arctic GN01 section ranged from below detection limit (0.04 pM) to 1.03 pM, with an average of 0.20 ± 0.16 pM (n = 269; Table 1). Similar mean concentrations and ranges have been reported for waters in the Canadian Arctic Archipelago, Nordic seas, and central Arctic Ocean (Andersson et al., 2008; Kirk et al., 2008; Sommar et al., 2007; St. Louis et al., 2007). Hg^0 distributions had nutrient-type profiles in ice-free waters, similar to other oceans (Bowman et al., 2015; Bowman et al., 2016; Cossa et al., 2011; Mason et al., 1995), but ice-covered waters had a surface maximum, which may be unique to polar seas (Fig. 5). Hg^0 in BSMW (0.25 ± 0.19 pM, n = 79) suggests it may be transported into the central Arctic Ocean from the Bering Strait and Chukchi shelf (Fig. 3B). It is possible that the broad shallow shelves host microbes possessing *merA*, a gene responsible for reducing Hg^{2+} to Hg^0 (Summers and Sugarman, 1974; Summers and Silver, 1978). Hg^0 in PML (0.21 ± 0.19 pM, n = 63) is similar to AW (0.21 ± 0.15 pM, n = 29), and deep waters contain lower levels. Average amounts of Hg^0 in CBDW (0.11 ± 0.06 pM, 21 ± 13% of HgT as Hg^0, n = 27) and EBDW (0.13 ± 0.03 pM, 25 ± 8%, n = 5) were comparable, despite a water mass age difference of > 200 years. This is in contrast to previous reports of decreasing Hg^0 with increasing water mass age (Bowman et al., 2015, 2016), suggesting that Hg^0 loss mechanisms are slower in cold, and deep polar waters.

Surface waters at ice-covered stations had the highest Hg^0 measured along the GN01 section (Fig. 7). Hg^0 in ice-covered surface waters (< 21 m, 0.37 ± 0.26 pM, n = 17) were greater than in ice-free surface waters (0.074 ± 0.050 pM, n = 15; p < 0.001; Fig. 7). Similar under-ice surface concentrations have been reported in the Arctic (Andersson et al., 2008), and greater levels have been documented in surface waters from the North Pacific, most likely due to a highly reductive environment (Mason et al., 1998). Ice-covered waters were supersaturated with Hg^0 (230 ± 228%; DiMento et al., 2019). Hg^0 was a larger fraction of HgT (24 ± 13%, n = 12) in ice-capped waters than in ice-free waters (12 ± 11%, n = 21; p = 0.001). Greater levels of Hg^0 under sea ice have been observed by others (St. Louis et al., 2007), and may be due to limited gas exchange between the PML and the atmosphere. It is unlikely that excess Hg^0 results from photoreduction of Hg (II), as sea ice reflects and attenuates much of the incident sunlight and light transmittance to surface waters is low (4–11%; Nicolaus et al., 2012). Photoreduction of Hg(II) is largely dependent on UV-B, which is expected to attenuate more than PAR (Qureshi et al., 2010). Microbial communities with the *merA* operon can reduce Hg^{2+} to Hg^0, and have been found in ice-covered Arctic waters (Poulain et al., 2007), however, *merA* was not found in the GN01 section (Bowman et al., In prep.). This suggests that microbial community diversity and irregular ice thickness and cover might explain Hg^0 variability at ice stations. In addition, leads and breaks in ice cover may allow for degassing and contribute to variable Hg^0 content in the PML (Fig. 7).

Unlike HgT, the TPD did not significantly influence Hg^0 in surface waters. Ice-covered waters within the TPD did not contain more Hg^0 (0.37 ± 0.30 pM, n = 9) than ice-covered waters outside of the TPD (0.35 ± 0.27 pM, n = 6; p = 1.0). But, if we consider the entire extent of the TPD (< 100 m) and not solely the surface waters, Hg^0 is affected by meteoric water. A correlation between the fraction of meteoric water and Hg^0 was found (r = 0.78, p = 0.0002), and the coefficient of determination suggests the meteoric water is not the only factor influencing Hg^0 concentration (r^2 = 0.60; Fig. 4). Ice and an influx of meteoric water influences Hg^0 in ice-covered surface waters of the TPD, suggesting that changes in ice cover and TPD flow path and time will impact surface Hg^0 in the Arctic Ocean.

3.4. Filtered MMHg

Monomethylmercury concentrations along the GN01 section ranged from below detection limit (0.020 pM) to 0.36 pM, and averaged

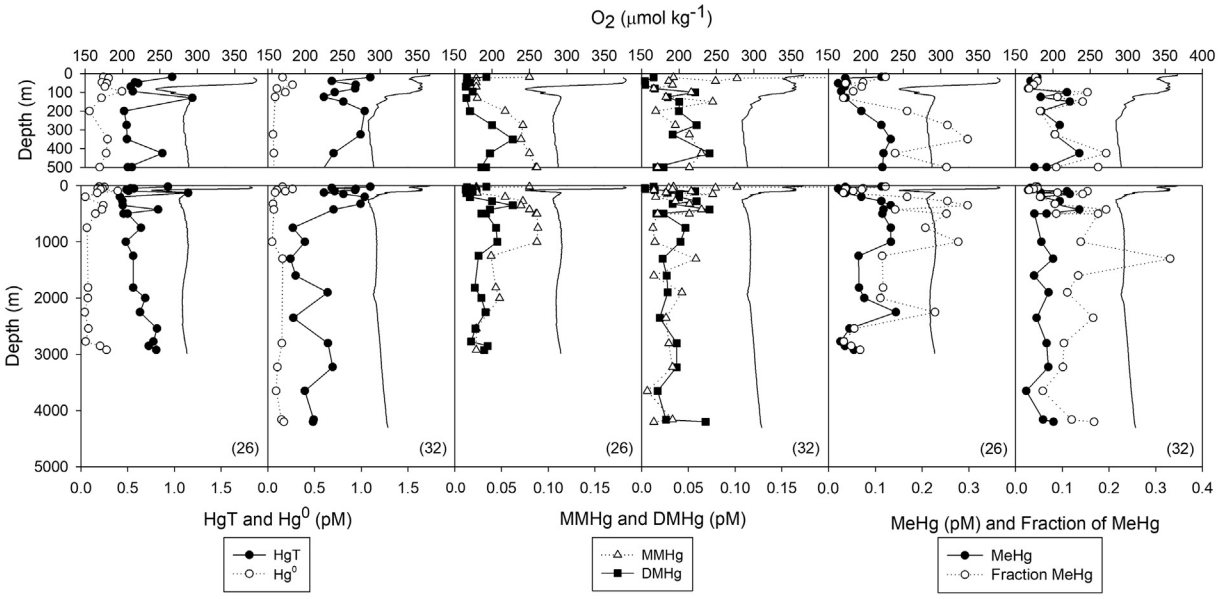

Fig. 5. Filtered mercury species at ice-covered stations in the Makarov (26; station depth of 2864 m) and Eurasian Basins (32; station depth of 4246 m). Top panel shows the upper 500 m and the lower figures show full depth profiles. Left panels contain filtered total mercury, elemental mercury, middle panels show filtered monomethylmercury and dimethylmercury, and right panels show total methylated mercury and the fraction of methylated mercury. All panels show dissolved oxygen (black line).

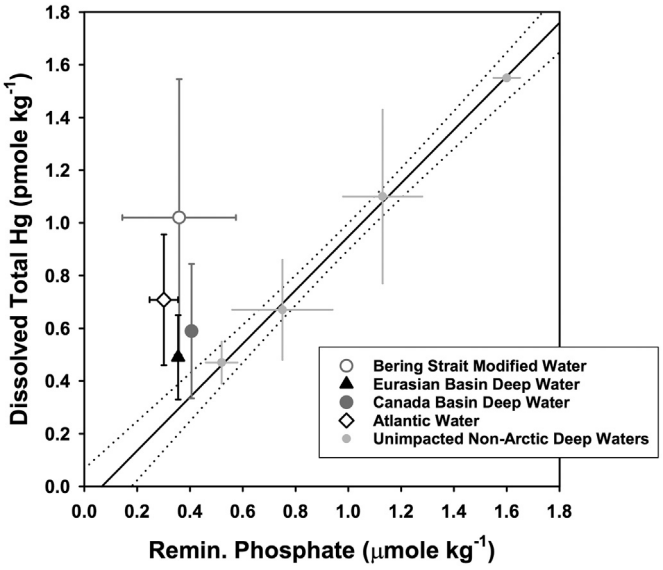

Fig. 6. Filtered total mercury (HgT) measured in the western Arctic Ocean, compared to remineralized phosphate. Bering Strait Modified Water and Eurasian Basin Deep Water have HgT:P ratios greater than those in unaffected water masses (HgT:P = 1.02 ± 0.03), suggesting they contain anthropogenic mercury. Canada Basin Deep Water and Atlantic Water lie within the 95% confidence interval of the HgT:P ratio. The four grey symbols along the regression line represent water masses without anthropogenic mercury (Lamborg et al., 2014).

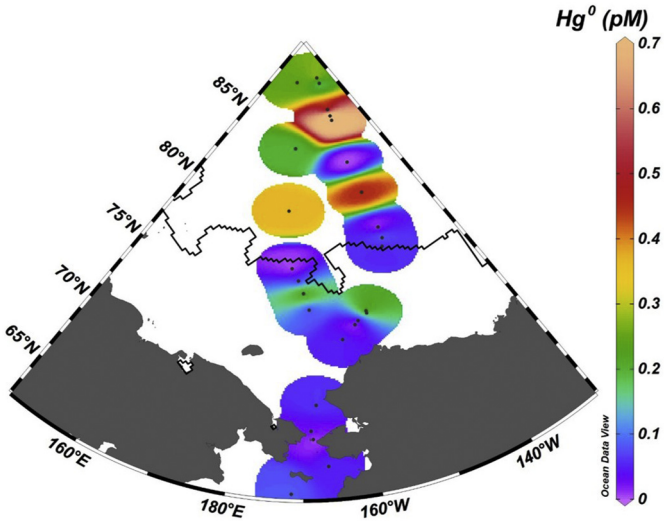

Fig. 7. Elemental Hg measurements at the shallowest depth sampled. The black line indicates the average ice extent for the month of September 2015 (Fetterer et al., 2017).

0.054 ± 0.050 pM (n = 164; Fig. 3C; Table 1). Surface water MMHg (0.064 ± 0.065 pM, n = 44, < 51 m) was about 30% lower than those observed in the Canadian Arctic Archipelago (0.09 ± 0.04 pM, Baya et al., 2015). Monomethylmercury averaged 0.047 ± 0.033 pM (n = 16) in CBDW and 0.030 ± 0.034 pM (n = 4) in EBDW. Several stations (i.e., 14, 26, 32, 48, 52, 57) had increased MMHg just above the ocean floor (Fig. 5), suggesting mobilization from sediments may be a source of MMHg to overlying water (Hammerschmidt et al., 2004; Hammerschmidt and Fitzgerald, 2006a; Hollweg et al., 2010). The fraction of HgT as MMHg and DMHg (%MeHg) averaged 12 ± 6% (n = 12) in the PML, 12 ± 9% (n = 19) in the halocline, 16 ± 10% (n = 21) in AW, and 18 ± 17% (n = 17) in deep water. Previous observations of unfiltered Arctic Ocean water in the central Arctic, Beaufort Sea, and the Archipelago observed a %MeHg maximum in the halocline (10–49%, 0.025–0.59 pM; Heimbürger et al., 2015; Wang et al., 2012; Wang et al., 2018). Our observations of %MeHg (sum of filtered and particulate) agree with previous reports, but we also observe a %MeHg maximum in AW (Fig. 5). An increase in %MeHg in AW might result from its circulation and interaction with the Arctic's broad shelves, where water masses might accumulate MeHg.

MMHg concentrations in the Arctic Ocean were unrelated to AOU, unlike the Pacific Ocean (Bowman et al., 2016; Munson et al., 2015; Sunderland et al., 2009), Southern Ocean (Cossa et al., 2011), and Mediterranean Sea (Cossa et al., 2009; Heimbürger et al., 2010). The

lack of correlation is likely due to the absence of an oxygen minimum zone, which is hypothesized to provide an anaerobic environment for methylating bacteria. Ice coverage in the Arctic Ocean leads to variable phytoplankton growth and activity (Arrigo and van Dijken, 2011; Arrigo et al., 2012), which might also explain the lack of correlation between MMHg and AOU, and also between MMHg and phytoplankton pigment concentration. Phytoplankton blooms occur under single year ice (Arrigo et al., 2012), but thick multi-year ice results in decreased light and low primary production (Arrigo and van Dijken, 2011). Primary production under ice tends to be at a shallower depth than in open water, which may explain irregularities in these biological proxies for MMHg distribution. The AOU in the Arctic is advected from the broad, nutrient-rich shelves, and has been linked with MMHg production over the shelf and in the Canadian Arctic Archipelago (Lehnherr et al., 2011). But the absence of correlation between MMHg and AOU in the central ocean maxima may indicate in situ MMHg production, rather than advection from the shelves (Heimbürger et al., 2015; Wang et al., 2012).

Neither the TPD, nor ice cover affect MMHg in surface water of the central Arctic Ocean (Fig. 3C). MMHg in the upper 20 m of the ice-covered TPD (0.069 ± 0.070 pM, $n = 13$) and ice-covered waters outside of the TPD (0.064 ± 0.024, $n = 3$) were not greater than ice-free waters (0.036 ± 0.009 pM, $n = 3$; $p = 0.0.3$, $p = 0.2$, respectively). MMHg in the upper 100 m of the TPD did not exhibit a relationship with meteoric water (Fig. 4). MMHg levels on the Siberian Shelf are unknown, but if we assume concentrations are similar to the Chuckchi Shelf (0.028 ± 0.007 pM, $n = 2$), and use a demethylation rate of 0.36 ± 0.09 d^{-1} (derived from polar marine waters, Lehnherr et al., 2011), and the estimated transport time of TPD water from the Siberian Shelf (6–12 months; Kipp et al., 2018), then we would expect all shelf derived MMHg to be decomposed before reaching the central Arctic Ocean. The delivery of nutrients by the TPD likely fertilizes both methylating and demethylating microbial communities, which may result in variable MMHg that does not correlate with the fraction of meteoric water. There is also the possibility of localized, under-ice microbial communities which methylate Hg, which might explain MMHg variability in the TPD.

MMHg in the western Arctic Ocean is less than the Atlantic Ocean (Bowman et al., 2015) and similar to the Pacific Ocean (Bowman et al., 2016; Table 1). One explanation for lower MMHg is the rate of demethylation in polar marine waters is relatively high (Lehnherr et al., 2011). Thus, while Hg methylation may be active by microbial communities under the ice and in the halocline, demethylation likely lowers the steady-state concentration of MMHg and leads to low MMHg throughout the western Arctic Ocean. Therefore, low MMHg concentrations in the western Arctic Ocean do not explain anomalous MMHg concentrations in Arctic animals, and measurements from this study suggest other regions should be studied for MMHg production and assimilation into the food chain.

3.5. DMHg

DMHg ranged from below the detection limit (0.012 pM) to 0.23 pM with an average concentration of 0.040 ± 0.029 pM ($n = 199$; Table 1). As with MMHg, DMHg concentrations were lower than those measured in either the North Atlantic (Bowman et al., 2015) or the eastern tropical Pacific (Bowman et al., 2016), but comparable to those measured in the Canadian Arctic (Baya et al., 2015; Kirk et al., 2008; St. Louis et al., 2007). The average ratio of MMHg:DMHg in the Arctic Ocean was 2.1 ± 2.5 ($n = 108$). The MMHg:DMHg ratio remained relatively consistent from the upper 150 m of the water column (3.0 ± 4.0, $n = 33$) through intermediate and deep waters (1.6 ± 1.4, $n = 57$; 1.7 ± 1.0, $n = 18$). Upper water column mean values are similar to North Pacific waters (Bowman et al., 2016; Hammerschmidt and Bowman, 2012), but much less than in the North Atlantic (Bowman et al., 2015). Meanwhile, the deep water mean ratio suggests that in the Arctic Ocean, DMHg is not necessarily the dominant methylated species below the thermocline, which has been found to be the case in other oceans (Cossa et al., 1997; Mason et al., 1993; Mason et al., 1995). DMHg concentrations were unrelated to pigment concentrations, AOU, N* (a proxy for denitrification), and P_{remin}. The mechanism for DMHg production is unknown, but if the primary source of DMHg were from MMHg methylation, low MMHg in the Arctic Ocean may limit DMHg.

Vertical distributions of DMHg in the Arctic Ocean (Figs. 3 and 5) had a similar shape to other oceans, with a low surface water average (0.024 ± 0.016 pM, $n = 21$), a subsurface maximum in the halocline (0.041 ± 0.024, $n = 45$), and homogenized levels below 1000 m, with similar average concentrations in EBDW (0.034 ± 0.019 pM, $n = 6$) and CBDW (0.030 ± 0.017, $n = 22$). The subsurface DMHg maxima is more prominent in the Canada Basin, and may be partially due to AW (0.041 ± 0.021 pM, $n = 28$; Figs. 3D, 5). Atlantic Water increases in density and circulates in a rim current, therefore it is possible the water mass accumulates nutrients beneficial for MMHg formation from the continental shelf, that are subsequently methylated to form DMHg. Interactions with the shelf may also allow AW to accumulate organic matter with reduced sulfide groups that are conducive to DMHg formation (Jonsson et al., 2016). The maximum follows the 300 μmol kg^{-1} oxygen contour, whereas in other oceans, the DMHg maximum occurs at depths with lower amounts of oxygen (Bowman et al., 2015, 2016).

Unlike Hg^0, DMHg did not exhibit a surface maxima under sea ice in the Arctic Ocean. As described above, the presence of sea ice prevents degassing of Hg^0, but DMHg was not observed to concentrate in water under the ice in an analogous way. Ice likely prohibits DMHg evasion, so some under ice processes must prevent the buildup of DMHg. Under ice communities are either incapable of forming DMHg or demethylation rates are similar in magnitude to methylation rates. Demethylation of DMHg may occur either via biotic processes, or photodecomposition that leaves Hg^0 either undisturbed or indistinguishable from high Hg^0 concentrations under the ice, or a combination of all these processes. The influx of young shelf water does not yield higher DMHg concentrations. The TPD had a negative effect on DMHg concentration, as fraction of meteoric water and DMHg are inversely related with a correlation coefficient of 0.69 (Fig. 4). An inverse relationship between DMHg and meteoric water supports the idea that DMHg is more likely to form in the marine water column as opposed to freshwater systems.

3.6. Particulate HgT

The average concentration of particulate HgT (HgT_{Part}) along the GN01 transect was 0.1 ± 0.1 pM ($n = 141$; Table 1). HgT_{Part} concentrations were greatest in surface waters, and declined with depth to about 1000 m, and were homogenous throughout deep waters (Fig. 8A). Profiles and average concentrations of HgT in the Arctic Ocean are not similar to those observed in the North Atlantic Ocean (Bowman et al., 2015; Mason et al., 1998) and eastern tropical South Pacific Ocean (Bowman et al., 2016; Table 1). The average for the Arctic Ocean is greater than other oceans studied presumably due to both broad shelves and riverine input, which supply HgT_{Part} to the central Arctic. The largest source of HgT_{Part} to the Arctic Ocean is BSMW which had a distinct shelf fingerprint consisting of tracers such as filtered Cd extending into the central Arctic Ocean (Personal communication, Laramie Jensen, Texas A&M, and Laura Whitmore, University of Southern Mississippi). Particulate HgT in BSMW (0.13 ± 0.15 pM, $n = 63$) is significantly greater than HgT_{part} in the central Arctic, including the TPD (0.04 ± 0.04, $n = 33$; $p < 0.001$). The relatively young age of the TPD and the combined shelf and riverine source would suggest high HgT_{Part} concentrations in the TPD. However, HgT_{Part} measured in the TPD (0.09 ± 0.05 pM, $n = 14$) is significantly lower than HgT_{Part} in the upper 100 m outside of the TPD (0.22 ± 0.21 pM, $n = 37$; $p = 0.019$). This is likely due to particles in BSMW, and those particles were accumulated on the shelf.

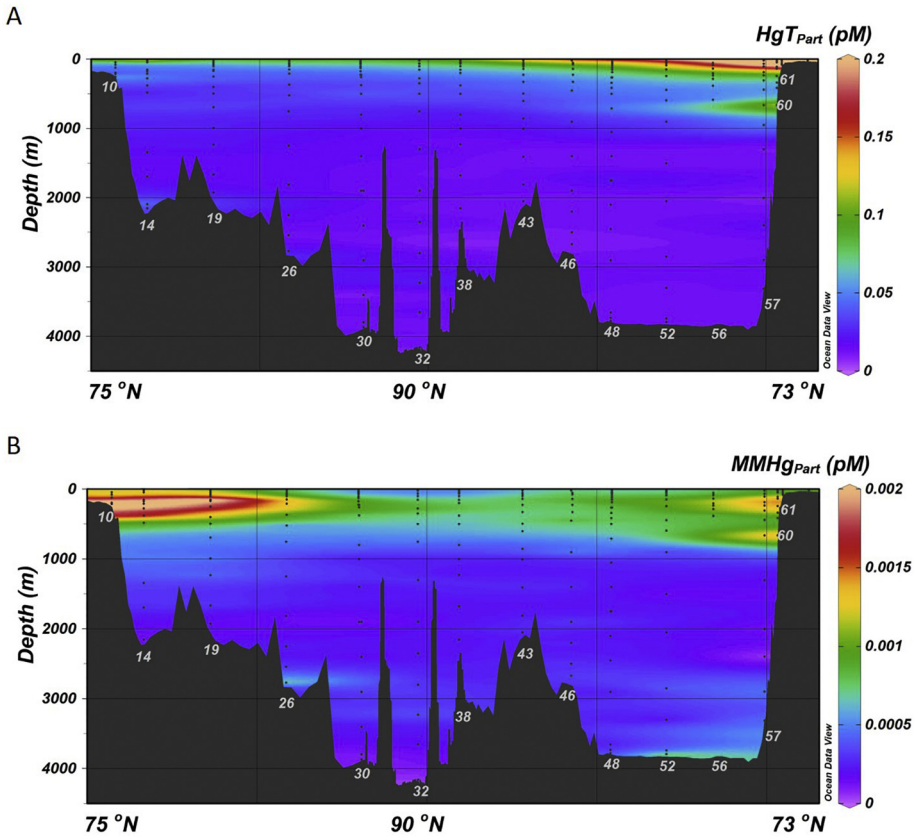

Fig. 8. Filtered particulate total Hg (HgT_{Part}, A) and particulate monomethyl-Hg ($MMHg_{Part}$, B) in the GN01 transect. Station numbers are denoted by numbers in the bathymetry, and black dots throughout the water column indicate sampling depth.

3.7. Particulate MMHg

Particulate MMHg ($MMHg_{Part}$) concentrations varied widely, and 93% of samples were below the detection limit (0.002 pM). The average concentration for $MMHg_{Part}$ in the Arctic was 0.004 ± 0.003 pM (n = 17), and $MMHg_{Part}$ constituted 0–86% of the HgT_{Part}. Mean measurements of Arctic $MMHg_{Part}$ are an order of magnitude greater than mean values for $MMHg_{Part}$ in the North Atlantic Ocean (Bowman et al., 2015) and the eastern tropical South Pacific Ocean (Bowman et al., 2016; Table 1). The average from this study is likely an order of magnitude greater due to the majority of samples falling below the detection limit, and thus the sample average is disproportionately weighted by $MMHg_{Part}$ concentrations from shelf particles and few quantifiable particles from the open ocean (Fig. 8B). Chukchi Shelf waters have high $MMHg_{Part}$ concentrations, and are advected with BSMW into the open ocean. These trends mirror those of HgT_{Part}, indicating sources of particulate MMHg and HgT to the Arctic are the Bering Strait and Chukchi Shelf. Some station profiles exhibited resuspension of $MMHg_{Part}$ in nephloid layers, but the magnitude of resuspension varied depending on the local bathymetry. The vertical distribution of $MMHg_{Part}$ was low in the surface, with a subsurface maxima and homogeneous below 1000 m, except for resuspension from the sediment or where water had recently interacted with a sill.

Particulate MMHg in the TPD was below detection limit, and lower than $MMHg_{Part}$ concentrations measured in the PML (0.003 ± 0.002 pM, n = 4). One possible explanation for differences in concentration might be a difference in particle lability due to the particle source, affecting $MMHg_{Part}$ to a greater extent than HgT_{Part}. Settling rate of particles from the Siberian Shelf might also be greater than that of particles from the Chukchi Shelf.

4. Conclusions

Four species of Hg were analyzed in seawater from the Bering Sea and Strait, Canada and Makarov Basins, and just over the Lomonosov Ridge in the Eurasian Basin in the western Arctic Ocean. Total Hg concentrations were the greatest in the Bering Sea and Strait and under ice in the TPD. Elemental Hg in surface water was greater under the ice than in ice-free waters, especially in the TPD. Methylated forms of Hg in water were greater over the shelf compared to open ocean, and vertical profiles exhibit a subsurface maxima in both MMHg and DMHg, neither of which were related to either oxygen consumption or nutrient levels. Unlike HgT and Hg^0, the TPD was not a source of MMHg or DMHg to the central Arctic Ocean. The Chukchi Shelf appears to be an important source of particulate HgT and MMHg to the Arctic, and may be an important part of the Arctic Hg food chain. All forms of filtered Hg in the Arctic Ocean had lower average concentrations than found in either the Atlantic or Pacific Oceans. Average particulate concentrations of HgT and MMHg were greater than those in either the Pacific or Atlantic Oceans, which was likely due to low concentrations in the open ocean, most of which were below detection limit. By itself, low MMHg in the western Arctic Ocean does not explain anomalously high Hg levels in Arctic animals.

Acknowledgments

We thank chief scientists David Kadko and William Landing; the Captain, officers, and crew of the U.S. Coast Guard cutter *Healy* (HLY1502). We thank the GEOTRACES sampling team: Greg Cutter, Kyle McQuiggan, Peter Morton, Sarah Rauschenberg, Gabi Weiss, Simone Moos, and Lisa Oswald; the pump team: Phoebe Lam, Maija Heller, Yang Xiang, Steven Pike, Erin Black, and Lauren Kipp; and the small boat operations, ice, and melt pond teams: Ana Aguilar-Islas, Rob

Rember, Neil Wyatt, and Chris Marsay. We thank Brian DiMento for sharing total gaseous mercury data. We thank Kim Vaeth and William Fitzgerald for looking at earlier versions of this draft and providing helpful feedback. We also thank Kelly Muterspaw, Kayla Haman, Kortney Mullen and Katelynn Alcorn for help in the lab. This work was funded by the U.S. National Science Foundation grants OCE-1434650, 1434653, and 1534315.

Filtered Hg (https://www.bco-dmo.org/dataset/738136) and particulate Hg datasets (https://www.bco-dmo.org/dataset/738307) are available for download from the Biological and Chemical Oceanography Data Management Office.

Declarations of Competing Interest

None.

Contributors and role of funding source

C.H.L. and C.R.H. designed the study. A.M.A, K.L.B. and C.H.L collected samples and did lab work. A.M.A. drafted the first draft of the manuscript. All authors contributed to the interpretation of results and manuscript writing. This work was funded by the U.S. National Science Foundation grants OCE-1434650, 1434653, and 1534315. NSF had no involvement in the project design, collection, analysis, or interpretation of this dataset.

References

Anderson, L.A., Sarmiento, J.L., 1994. Redfield ratios of remineralization determined by nutrient data analysis. Glob. Biogeochem. Cycles 8, 65–80.
Andersson, M.E., Sommar, J., Gårdfeldt, K., Lindqvist, O., 2008. Enhanced concentrations of dissolved gaseous mercury in the surface waters of the Arctic Ocean. Mar. Chem. 110, 190–194.
Arrigo, K.R., van Dijken, G.L., 2011. Secular trends in Arctic Ocean net primary production. J. Geophys. Res. 116, C09011.
Arrigo, K.R., Perovich, D.K., Pickart, R.S., Brown, Z.W., van Dijken, G.L., Lowry, K.E., Mills, M.M., Palmer, M.A., Balch, W.M., Bahr, F., Bates, N.R., Benitez-Nelson, C., Bowler, B., Brownlee, E., Ehn, J.K., Frey, K.E., Garley, R., Laney, S.R., Lubelczyk, L., Mathis, J., Matsuoka, A., Mitchell, B.G., Moore, G.W.K., Ortega-Retuerta, E., Pal, S., Polashenski, C.M., Reynolds, R.A., Schieber, B., Sosik, H.M., Stephens, M., Swift, J.H., 2012. Massive phytoplankton blooms under Arctic sea ice. Science 336, 1408.
Barrie, L., Flack, E., Gregor, D.J., Iversen, T., Loeng, H., Macdonald, R., Pfirman, S., Skotvold, T., Wartena, E., 1998. The influence of physical and chemical processes on contaminant transport into and within the Arctic. In: Gregor, D.J., Loeng, H., Barrie, L. (Eds.), AMAP Assessment Report: Arctic Pollution Issues. Arctic Monitoring and Assessment Programme, Oslo, Norway, pp. 25–116.
Baya, P.A., Hollinsworth, J.L., Hintelmann, H., 2013. Evaluation and optimization of solid adsorbents for the sampling of gaseous methylated mercury species. Anal. Chim. Acta 786, 61–69.
Baya, P.A., Gosselin, M., Lehnherr, I., St. Louis, V.L., Hintelmann, H., 2015. Determination of monomethylmercury and dimethylmercury in the Arctic marine boundary layer. Environ. Sci. Technol. 49, 223–232.
Beattie, S.A., Armstrong, D., Chaulk, A., Comte, J., Gosselin, M., Wang, F., 2014. Total and methylated mercury in Arctic multiyear sea ice. Environ. Sci. Technol. 48, 5575–5582.
Bishop, J.K., Lam, P.J., Wood, T.J., 2012. Getting good particles: accurate sampling of particles by large volume in-situ filtration. Limnol. Oceanogr. Methods 10, 681–710.
Bloom, N., 1989. Determination of pictogram levels of methylmercury by aqueous phase ethylation, followed by cryogenic gas chromatography with cold vapour atomic fluorescence detection. Can. J. Fish. Aquat. Sci. 46, 1131–1140.
Bloom, N.S., Crecelius, E.A., 1983. Determination of mercury in seawater at sub-nanogram per liter levels. Mar. Chem. 14, 49–59.
Bloom, N., Fitzgerald, W.F., 1988. Determination of volatile mercury species at the picogram level by low-temperature gas chromatography with cold-vapour atomic fluorescence detection. Anal. Chim. Acta 208, 151–161.
Bowman, K.L., Hammerschmidt, C.R., 2011. Extraction of monomethylmercury from seawater for low-femtomolar determination. Limnol. Oceanogr. Methods 9, 121–128.
Bowman, K.L., Hammerschmidt, C.R., Lamborg, C.H., Swarr, G., 2015. Mercury in the North Atlantic Ocean: the U.S. GEOTRACES zonal and meridional sections. Deep-Sea Res. II 116, 251–261.
Bowman, K.L., Hammerschmidt, C.R., Lamborg, C.H., Swarr, G.J., Agather, A.M., 2016. Distribution of mercury species across a zonal section of the eastern tropical South Pacific Ocean (U.S. GEOTRACES GP16). Mar. Chem. 186, 156–166.
Bowman, K.L., Collins, E., Agather, A.M., Lamborg, C.H., Hammerschmidt, C.R., Christensen, G., Elias, D., Podar, M., Kaul, D., Dupont, C., Saito, M.A., 2019. Presence and Distribution of Mercury-Cycling Genes in the Arctic and Pacific Oceans and their Relationship to Mercury Speciation. (In preparation).
Coquery, M., Cossa, D., Martin, J.M., 1995. The distribution of dissolved and particulate mercury in three Siberian estuaries and adjacent Arctic coastal waters. Water Air Soil Pollut. 80, 653–664.
Cossa, D., Martin, J.-M., Takayanagi, K., Sanjuan, J., 1997. The distribution and cycling of mercury species in the western Mediterranean. Deep-Sea Res. II 44 (3–4), 721–740.
Cossa, D., Averty, B., Pirrone, N., 2009. The origin of methylmercury in open Mediterranean waters. Limnol. Oceanogr. 54 (3), 837–844.
Cossa, D., Heimbürger, L.-E., Lannuzel, D., Rintoul, S.R., Butler, E.C.V., Bowie, A.R., Averty, B., Watson, R.J., Remenyi, T., 2011. Mercury in the Southern Ocean. Geochim. Cosmochim. Acta 75, 4037–4052.
Cutter, G.A., Bruland, K.W., 2012. Rapid and noncontaminating sampling system for trace elements in global ocean surveys. Limnol. Oceanogr. Methods 10, 425–436.
Dastoor, A.P., Durnford, D.A., 2014. Arctic Ocean: is it a sink or a source of atmospheric mercury? Environ. Sci. Technol. 48, 1707–1717.
Dietz, R., Pacyna, J., Thomas, D.J., Asmund, G., Gordeev, V.V., Johansen, P., Kimstach, V., Lockhart, L., Pfirman, S., Riget, F., Shaw, G., Wagemann, R., White, M., 1998. Heavy metals. In: Dietz, R., Pacyna, J., Thomas, D.J. (Eds.), AMAP Assessment Report: Arctic Pollution Issues. Arctic Monitoring and Assessment Programme, Oslo, Norway, pp. 373–453.
Dietz, R., Outridge, P.M., Hobson, K.A., 2009. Anthropogenic contributions to mercury levels in present-day Arctic animals—a review. Sci. Total Environ. 407, 6120–6131.
Dijkstra, J.A., Buckman, K.L., Ward, D., Evans, D.W., Dionne, M., Chen, C.Y., 2013. Experimental and natural warming elevates mercury concentrations in estuarine fish. PLoS One 8 (3), e58401.
DiMento, B.P., Mason, R.P., Brooks, S., Moore, C., 2019. The impact of sea ice on the air-sea exchange of mercury in the Arctic Ocean. Deep-Sea Res. II 144, 28–38.
Fetterer, F., Knowles, K., Meier, W., Savoie, M., Windnagel, A.K., 2017. *Sea Ice Index, Version 3*. Monthly Sea Ice Extent, September 2015. NSDIC: National Snow and Ice Data Center, Boulder, CO, USA. https://doi.org/10.7265/N5K072F8. updated daily. Data set. (Accessed 04/17/16).
Fisher, J.A., Jacob, D.J., Soerensen, A.L., Amos, H.M., Steffen, A., Sunderland, E.M., 2012. Riverine source of Arctic Ocean mercury inferred from atmospheric observations. Nat. Geosci. 5, 499–504.
Fisher, J.A., Jacob, D.J., Sorensen, A.L., Amos, H.M., Corbitt, E.S., Streets, D.G., Wang, Q., Yantosca, R.M., Sunderland, E.M., 2013. Factors driving mercury variability in the Arctic atmosphere and ocean over the past 30 years. Glob. Biogeochem. Cycles 27, 1226–1235.
Fitzgerald, W.F., Gill, G.A., 1979. Subnanogram determination of mercury by two-stage gold amalgamation and gas phase detection applied to atmospheric analysis. Anal. Chem. 51 (11), 1714–1720.
Fitzgerald, W.F., Engstrom, D.R., Mason, R.P., Nater, E.A., 1998. The case for atmospheric mercury contamination in remote areas. Environ. Sci. Technol. 32 (1), 1–7.
Fitzgerald, W.F., Engstrom, D.R., Lamborg, C.H., Tseng, C.-M., Balcom, P.H., Hammerschmidt, C.R., 2005. Modern and historic atmospheric mercury fluxes in Northern Alaska: global sources and Arctic depletion. Environ. Sci. Technol. 39, 557–568.
Gionfriddo, C.M., Tate, M.T., Wick, R.R., Schultz, M.B., Zelma, A., Thelen, M.P., Schofield, R., Krabbenhoft, D.P., Holt, K.E., Moreau, J.W., 2016. Microbial mercury methylation in Antarctic sea ice. Nat. Microbiol. 16127. https://doi.org/10.1038/NMICROBIOL2016.127.
Gordienko, P.A., Laktionov, A.F., 1969. Circulation and physics of the Arctic Basin waters. In: Gordon, A.L., Baker, F.W.G. (Eds.), Oceanography: Annals of the International Geophysical Year. 46. Pergamon Press, London, pp. 94–112.
Grandjean, P., Weihe, P., Needham, L.L., Burse, V.W., Patterson Jr., D.G., Sampson, E.J., Jørgensen, P.J., Vahter, M., 1995. Relation of a seafood diet to mercury, selenium, arsenic, and polychlorinated biphenyl and other organochlorine concentrations in human milk. Environ. Res. 71, 29–38.
Ha, E., Basu, N., Bose-O'Reilly, S., Dórea, J.G., McSorley, E., Sakamoto, M., Chan, H.M., 2017. Current progress on understanding the impact of mercury on human health. Environ. Res. 152, 419–433.
Hammerschmidt, C.R., Bowman, K.L., 2012. Vertical methylmercury distribution in the subtropical North Pacific Ocean. Mar. Chem. 132–133, 77–82.
Hammerschmidt, C.R., Fitzgerald, W.F., 2006a. Methylmercury cycling in sediments on the continental shelf of southern New England. Geochim. Cosmochim. Acta 70, 918–930.
Hammerschmidt, C.R., Fitzgerald, W.F., 2006b. Bioaccumulation and trophic transfer of methylmercury in Long Island Sound. Arch. Environ. Contam. Toxicol. 51, 416–424.
Hammerschmidt, C.R., Fitzgerald, W.F., Lamborg, C.H., Balcom, P.H., Visscher, P.T., 2004. Biogeochemistry of methylmercury in sediments of Long Island Sound. Mar. Chem. 90, 31–52.
Hammerschmidt, C.R., Bowman, K.L., Tabatchnick, M.D., Lamborg, C.H., 2011. Storage bottle material and cleaning for determination of total mercury in seawater. Limnol. Oceanogr. Methods 9, 426–431.
Hatta, M., Measures, C., 2018. GEOTRACES Arctic Section: Shipboard Determination of Key Trace Elements. BCO-DMO Dataset. https://www.bco-dmo.org/project/757016.
Heimbürger, L.-E., Cossa, D., Marty, J.-C., Migon, C., Averty, B., Dufour, A., Ras, J., 2010. Methyl mercury distributions in relation to the presence of nano- and picoplankton in an oceanic water column (Ligurian Sea, North-western Mediterranean). Geochim. Cosmochim. Acta 74, 5549–5559.
Heimbürger, L.-E., Sonke, J.E., Cossa, D., Point, D., Lagane, C., Laffont, L., Galfond, B.T., Nicolaus, M., Rabe, B., Rutgers van der Loeff, M., 2015. Shallow methylmercury production in the marginal sea ice zone of the central Arctic Ocean. Sci. Rep. 5, 10318. https://doi.org/10.1038/srep10318.
Hollweg, T.A., Gilmour, C.C., Mason, R.P., 2010. Mercury and methylmercury cycling in sediments of the mid-Atlantic continental shelf and slope. Limnol. Oceanogr. 55 (6), 2703–2722.
Horowitz, H.M., Jacob, D.J., Zhang, Y., Dibble, T.S., Slemr, F., Amos, H.M., Schmidt, J.A., Corbitt, E.S., Marais, E.A., Sunderland, E.M., 2017. A new mechanism for atmospheric mercury redox chemistry: implications for the global mercury budget. Atmos. Chem. Phys. 17, 6353–6371.
Jakobsson, M., 2002. Hypsometry and volume of the Arctic Ocean and its constituent seas. Geochem. Geophys. Geosyst. 3 (5), 1–18.
Jonsson, S., Mazrui, N.M., Mason, R.P., 2016. Dimethylmercury formation mediated by

inorganic and organic reduced sulfur surfaces. Sci. Rep. 6, 27958. https://doi.org/10.1038/srep27958.
Karagas, M.R., Choi, A.L., Oken, E., Horvat, M., Schoeny, R., Kamai, E., Cowell, W., Grandjean, P., Korrick, S., 2012. Evidence on the human health effects of low-level methylmercury exposure. Environ. Health Perspect. 120 (6), 799–806.
Kipp, L.E., Charette, M.A., Moore, W.S., Henderson, P.B., Rigor, I.G., 2018. Increased fluxes of shelf-derived materials to the Central Arctic Ocean. Sci. Adv. 4, eaao1302.
Kirk, J.L., St. Louis, V.L., Sharp, M.J., 2006. Rapid reduction and reemission of mercury deposited into snowpacks during atmospheric mercury depletion events at Churchill, Manitoba. Canada. Environ. Sci. Technol. 40, 7590–7596.
Kirk, J.L., St. Louis, V.L., Hintelmann, H., Lehnherr, I., Else, B., Poissant, L., 2008. Methylated mercury species in marine waters of the Canadian High and Sub Arctic. Environ. Sci. Technol. 42, 8367–8373.
Klunder, M.B., Bauch, D., Laan, P., de Baar, H.J.W., van Heuven, S., Ober, S., 2012. Dissolved iron in the Arctic shelf seas and surface waters of the central Arctic Ocean: impact of Arctic river water and ice-melt. J. Geophys. Res. 117, C01027.
Lamborg, C.H., Hammerschmidt, C.R., Gill, G.A., Mason, R.P., Gichuki, S., 2012. An intercomparison of procedures for the determination of total mercury in seawater and recommendations regarding mercury speciation during GEOTRACES cruises. Limnol. Oceanogr. Methods 10, 90–100.
Lamborg, C.H., Hammerschmidt, C.R., Bowman, K.L., Swarr, G.J., Munson, K.M., Ohnemus, D.C., Lam, P.J., Heimbürger, L.-E., Rijkenberg, M.J.A., Saito, M.A., 2014. A global ocean inventory of anthropogenic mercury based on water column measurements. Nature 512, 65–68.
Lammers, R.B., Shiklomanov, A.I., Vörösmarty, C.J., Fekete, B.M., Peterson, B.J., 2001. Assessment of contemporary Arctic river runoff based on observational discharge records. J. Geophys. Res. 106 (D4), 3321–3334.
Laurier, F.J.G., Mason, R.P., Gill, G.A., Whalin, L., 2004. Mercury distributions in the North Pacific Ocean—20 years of observations. Mar. Chem. 90, 3–19.
Lavoie, R.A., Jardine, T.D., Chumchal, M.M., Kidd, K.A., Campbell, L.M., 2013. Biomagnification of mercury in aquatic food webs: a worldwide meta-analysis. Environ. Sci. Technol. 47, 13385–13394.
Lehnherr, I., St. Louis, V.L., Hintelmann, H., Kirk, J.L., 2011. Methylation of inorganic mercury in polar marine waters. Nat. Geosci. 4, 298–302.
Lindberg, S.E., Brooks, S., Lin, C.-J., Scott, K.J., Landis, M.S., Stevens, R.K., Goodsite, M., Richter, A., 2002. Dynamic oxidation of gaseous mercury in the Arctic troposphere at polar sunrise. Environ. Sci. Technol. 36, 1245–1256.
Macdonald, R.W., Harner, T., Fyfe, J., 2005. Recent climate change in the Arctic and its impact on contaminant pathways and interpretation of temporal trend data. Sci. Total Environ. 342, 5–86.
Mahaffey, K.R., Clickner, R.P., Jeffries, R.A., 2009. Adult women's blood mercury concentrations vary regionally in the United States: association with patterns of fish consumption (NHANES 1999–2004). Environ. Health Perspect. 117 (1), 47–53.
Mason, R.P., Fitzgerald, W.F., Hurley, J., Hanson, A.K., Donaghay, P.L., Sieburth, J.M., 1993. Mercury biogeochemical cycling in a stratified estuary. Limnol. Oceanogr. 38 (6), 1227–1241.
Mason, R.P., Rolfhus, K.R., Fitzgerald, W.F., 1995. Methylated and elemental mercury cycling in surface and deep ocean waters of the North Atlantic. Water Air Soil Pollut. 80, 665–677.
Mason, R.P., Rolfhus, K.R., Fitzgerald, W.F., 1998. Mercury in the North Atlantic. Mar. Chem. 61, 37–53.
Mason, R.P., Choi, A.L., Fitzgerald, W.F., Hammerschmidt, C.R., Lamborg, C.H., Soerensen, A.L., Sunderland, E.M., 2012. Mercury biogeochemical cycling in the ocean and policy implications. Environ. Res. 119, 101–117.
McClelland, J.W., Déry, S.J., Peterson, B.J., Holmes, R.M., Wood, E.F., 2006. A pan-arctic evaluation of changes in river discharge during the latter half of the 20th century. Geophys. Res. Lett. 33, 1–4 L06715.
Mergler, D., Anderson, H.A., Hing Man Chan, L., Mahaffey, K.R., Murray, M., Sakamoto, M., Stern, A.H., 2007. Methylmercury exposure and health effects in humans: a worldwide concern. Ambio 36 (1), 3–11.
Munson, K.M., Babi, D., Lamborg, C.H., 2014. Determination of monomethylmercury from seawater with ascorbic acid-assisted direct ethylation. Limol. Oceanogr. Methods 12, 1–9.
Munson, K.M., Lamborg, C.H., Swarr, G.J., Saito, M.A., 2015. Mercury species concentrations and fluxes in the Central Tropical Pacific Ocean. Glob. Biogeochem. Cycles 29, 656–676.
Nicolaus, M., Katlein, C., Maslanik, J., Hendricks, S., 2012. Changes in Arctic sea ice result in increasing light transmittance and absorption. Geophys. Res. Lett. 39, L24501.
Oskarsson, A., Schültz, A., Skerfving, S., Hallén, I.P., Ohlin, B., Lagerkvist, B.J., 1996. Total and inorganic mercury in breast milk in relation to fish consumption and amalgam fillings in lactating women. Arch. Environ. Health 51 (3), 234–241.
Outridge, P.M., Macdonald, R.W., Wang, F., Stern, G.A., Dastoor, A.P., 2008. A mass balance inventory of mercury in the Arctic Ocean. Environ. Chem. 5, 89–111.
Pasqualini, A., Schlosser, P., Newton, R., Koffman, T.N., 2017. U.S. GEOTRACES artic Section Ocean water hydrogen and oxygen stable isotope analyses (version 1.0). Data set. IEDA. https://doi.org/10.1594/IEDA/100633.
Peterson, B.J., Holmes, R.M., McClelland, J.W., Vörösmarty, C.J., Lammers, R.B., Shiklomanov, A.I., Shiklomanov, I.A., Rahmstorf, S., 2002. Increasing river discharge to the Arctic Ocean. Science 298, 2171–2173.
Poulain, A.J., Ní Chadhain, S.M., Ariya, P.A., Amyot, M., Garcia, E., Campbell, P.G.C., Zylstra, G.J., Barkay, T., 2007. Potential for mercury reduction by microbes in the high Arctic. Appl. Environ. Microbiol. 73 (7), 2230–2238.
Qureshi, A., O'Driscoll, N.J., MacLeod, Neuhold, Y.-M., Hungerbühler, K., 2010. Photoreactions of mercury in surface ocean water: gross reaction kinetics and possible pathways. Environ. Sci. Technol. 44 (2), 644–649.
Roach, A.T., Aagaard, K., Pease, C.H., Salo, S.A., Weingartner, T., Pavlov, V., Kulakov, M., 1995. Direct measurements of transport and water properties through the Bering Strait. J. Geophys. Res. 100 (9), 18443–18457.
Rudels, B., 2001. Arctic Basin circulation. In: Steele, J.H., Thorpe, S.A., Turekian, K.K. (Eds.), Encyclopedia of Ocean Sciences. Elsevier Science Ltd, Oxford, UK, pp. 177–187.
Schartup, A.T., Balcom, P.H., Soerensen, A.L., Gosnell, K.J., Calder, R.S., Mason, R.P., Sunderland, E.M., 2015. Freshwater discharges drive high levels of methylmercury in Arctic marine biota. Proc Natl Acad Sci U S A. 112 (38), 11789–11794.
Scheuhammer, A., Braune, B., Chan, H.M., Frouin, H., Krey, A., Letcher, R., Loseto, L., Noël, M., Ostertag, S., Ross, P., Wayland, M., 2015. Recent progress on our understanding of the biological effects of mercury in fish and wildlife in the Canadian Arctic. Sci. Total Environ. 509–510, 91–103.
Schlosser, P., Kromer, B., Ekwurzel, B., Bönisch, G., McNichol, A., Schneider, R., von Reden, K., Östlund, H.G., Swift, J.H., 1997. The first trans-Arctic ^{14}C section: comparison of the mean ages of the deep waters in the Eurasian and Canadian basins of the Arctic Ocean. Nuc. Instr. And Meth. in Phys. Res. B 123, 431–437.
Schroeder, W.H., Anlauf, K.G., Barrie, L.A., Lu, J.Y., Steffen, A., Schneeberger, D.R., Berg, T., 1998. Arctic springtime depletion of mercury. Nature 394, 331–332.
Schuster, P.F., Schaefer, K.M., Aiken, G.R., Antweiler, R.C., Dewild, J.F., Gryziec, J.D., Gusmeroli, A., Hugelius, G., Jafarov, E., Krabbenhoft, D.P., Liu, L., Herman-Mercer, N., Mu, C., Roth, D.A., Schaefer, T., Striegl, R.G., Wickland, K.P., Zhang, T., 2018. Permafrost stores a globally significant amount of mercury. Geophys. Res. Lett. 45, 1463–1471.
Sheehan, M.C., Burke, T.A., Navas-Acien, A., Breysse, P.N., McGready, J., Fox, M.A., 2014. Global methylmercury exposure from seafood consumption and risk of developmental neurotoxicity: a systematic review. Bull. World Health Organ. 92 (4), 254–269F.
Slemr, F., Langer, E., 1992. Increase in global atmospheric concentrations of mercury inferred from measurements over the Atlantic Ocean. Nature 355, 434–437.
Slemr, F., Schuster, G., Seiler, W., 1985. Distribution, speciation, and budget of atmospheric mercury. J. Atmos. Chem. 3, 407–434.
Soerensen, A.L., Jacob, D.J., Schartup, A.T., Fisher, J.A., Lehnherr, I., St. Louis, V.L., Heimbürger, L.-E., Sonke, J.E., Krabbenhoft, D.P., Sunderland, E.M., 2016. A mass budget for mercury and methylmercury in the Arctic Ocean. Glob. Biogeochem. Cycles 30. https://doi.org/10.1002/2015GB005280.
Sommar, J., Wängberg, I., Berg, T., Gårdfelt, K., Munthe, J., Richter, A., Urba, A., Wittrock, F., Schroeder, W.H., 2007. Circumpolar transport and air-surface exchange of atmospheric mercury at Ny-Ålesund (79° N), Svalbard, spring 2002. Atmos. Chem. Phys. 7, 151–166.
St. Louis, V.L., Hintelmann, H., Graydon, J.A., Kirk, J.L., Barker, J., Dimock, B., Sharp, M.J., Lehnherr, I., 2007. Methylated mercury species in Canadian High Arctic marine surface waters and snowpacks. Environ. Sci. Technol. 41, 6433–6441.
St. Pierre, K.A., St. Louis, V.L., Kirk, J.L., Lehnherr, I., Wang, S., La Farge, C., 2015. Importance of open marine waters to the enrichment of total mercury and monomethylmercury in lichens in the Canadian High Arctic. Environ. Sci. Technol. 49, 5930–5938.
Steffen, A., Douglas, T., Amyot, M., Ariya, P., Aspmo, K., Berg, T., Bottenheim, J., Brooks, S., Cobbett, F., Dastoor, A., Dommergue, A., Ebinghaus, R., Ferrari, C., Kardfeldt, K., Goodsite, M.E., Lean, D., Poulain, A., Scherz, C., Skov, H., Sommar, J., Temme, C., 2007. A synthesis of atmospheric mercury depletion event chemistry linking atmosphere, snow and water. Atmos. Chem. Phys. Discuss. 7, 10837–10931.
Summers, A.O., Silver, S., 1978. Microbial transformations of metals. Annu. Rev. Microbiol. 32, 637–672.
Summers, A.O., Sugarman, L.I., 1974. Cell-free mercury(II)-reducing activity in a plasmid-bearing strain of *Escherichia coli*. J. Bacteriol. 119 (1), 242–249.
Sunderland, E.M., 2007. Mercury exposure from domestic and imported estuarine and marine fish in the U.S. seafood market. Environ. Health Perspect. 115 (2), 235–242.
Sunderland, E.M., Krabbenhoft, D.P., Moreau, J.W., Strode, S.A., Landing, W.M., 2009. Mercury sources, distribution, and bioavailability in the North Pacific Ocean: insights from data and models. Glob. Biogeochem. Cycles 23, GB2010. https://doi.org/10.1029/2008GB003425.
Swain, E.B., Engstrom, D.R., Brigham, M.E., Henning, T.A., Brezonik, P.L., 1992. Increasing rates of atmospheric mercury deposition in midcontinental North America. Science 257, 784–787.
Talley, L.D., Pickard, G.L., Emery, W.J., Swift, J.H., 2011. Arctic Ocean and Nordic seas. In: Talley, L.D. (Ed.), Descriptive Physical Oceanography, 6 Ed. Academic Press, London, pp. 401–436.
Tseng, C.-M., Hammerschmidt, C.R., Fitzgerald, W.F., 2004. Determination of methylmercury in environmental matrixes by on-line flow injection and atomic fluorescence spectrometry. Anal. Chem. 76 (23), 7131–7136.
Van Oostdam, J., Donaldson, S.G., Feeley, M., Arnold, D., Ayotte, P., Bondy, G., Chan, L., Dewaily, É., Furgal, C.M., Kuhnlein, H., Loring, E., Muchle, G., Myles, E., Receveur, O., Tracy, B., Gill, U., Kalhok, S., 2005. Human health implications of environmental contaminants in Arctic Canada: a review. Sci. Total Environ. 351–352, 165–246.
Wang, F., Macdonald, R.W., Armstrong, D.A., Stern, G.A., 2012. Total and methylated mercury in the Beaufort Sea: the role of local and recent organic remineralization. Environ. Sci. Technol. 46, 11821–11828.
Wang, K., Munson, K.M., Beaupré-Laperrière, A., Mucci, A., Macdonald, R.W., Wang, F., 2018. Subsurface seawater methylmercury maximum explains biotic mercury concentrations in the Canadian Arctic. Sci. Rep. 8, 14465. https://doi.org/10.1038/s41598-018-32760-0.
Zhang, Y., Jacob, D.J., Dutkiewicz, S., Amos, H.A., Long, M.S., Sunderland, E.M., 2015. Biogeochemical drivers of the fate of riverine mercury discharged to the global and Arctic oceans. Global Biogeochm. Cycles 29, 854–864.